Supplementary data: An ER-peroxisome tether exerts peroxisome population control in yeast

Expanded Materials and Methods

Plasmid and yeast strain construction

The open reading frame (ORF) of *PEX3* and 509 bp of its 5′-flanking region were cloned into the centromeric plasmid pYC6/CT (Invitrogen, Grand Island, NY) and used as a template for site-directed mutagenesis to introduce individually the six point mutations of the *pex3-1* allele (Munck *et al.*, 2009) using the Quick Change II Site-Directed Mutagenesis Kit (Agilent Technologies, Santa Clara, CA). Each mutation was verified by DNA sequencing. All *pex3* mutants used in this study are listed in Supplementary Table S2. Strains transformed with pYC6/CT were cultured in YPD medium supplemented with 100 μg Blasticidin S/ml.

For yeast two-hybrid analysis (Ishikawa *et al.*, 2003), PCR products encoding full-length Inp1p and a.a. 51-441 of wild-type and mutant Pex3 proteins were cloned in-frame and downstream of both the activation domain (AD) and the DNA-binding domain (BD) of the *GAL4* transcriptional activator in plasmids pGAD424 and pGBT9 (Clontech, Mountain View, CA), respectively. *S. cerevisiae* strains *SFY526* and *HF7c* transformed with the plasmids were used to measure β-galactosidase activity and cell growth, respectively. Cells were cultured in SM lacking leucine and tryptophan.

To construct a galactose-inducible *TOM70-INP1* expression system, the *TOM70* ORF and a 3′-linker encoding a polyglycine stretch, were cloned in-frame with the *INP1* ORF

containing a single hemagglutinin (HA) epitope at its 3′-end into pYC6/CT. Each part of the fusion construct was also cloned individually into pYC6/CT.

A galactose-inducible, photoconvertible fluorescent peroxisomal reporter was constructed by first inserting sequence encoding 3 copies of Dendra2 (3×Dendra2) obtained by BamHI/XhoI digestion of plasmid pKW2008 (a kind gift of Dr. Karsten Weis, University of California, Berkeley) into pYC6/CT. The ORF of the *POT1* gene coding for the peroxisomal enzyme thiolase and a 3′-polyglycine linker were then inserted upstream and in-frame with the 3×Dendra2 cassette.

An Inp2p-mCerulean expression system was constructed by cloning a DNA fragment consisting of the *INP2* ORF and 502 bp of its 5′-UTR, together a with 3′-polyglycine linker, upstream and in-frame with sequence coding for mCerulean (Rizzo *et al.*, 2004) into pYC6/CT.

A plasmid system for constitutive low-, intermediate-, and high-level expression of the *INP1* gene was constructed by cloning promoter sequences corresponding to 500 bp of the *INP1* and *CAN1* 5′-UTRs, as well as *TEF* promoter sequence corresponding to bp 411-795 of pFA6a-3HA-His3MX6 (Longtine *et al.*, 1998) into pYC6/CT. For microscopic observation of Inp1p levels, the *INP1* ORF and a 3′-polyglycine linker were cloned upstream and in-frame with sequence coding for GFP into the pYC6/CT-derived vectors. For immunodetection of Inp1p, the *INP1* ORF containing an HA-epitope was inserted into the vectors.

Yeast strains expressing genomically integrated *INP1*-3×GFP were obtained by a two-step, *Delitto perfetto* transformation strategy (Storici and Resnick, 2006). In the first step, a counter-selectable CORE-UK cassette was inserted by homologous recombination into the 3′-region of the

INP1 gene. The CORE-UK cassette was replaced in the second step by transformation with an *INP1*-specific 3×GFP cassette, followed by counter-selection on 5-FOA plates. The 3×GFP cassette was constructed by insertion of three copies of an improved version of GFP (GFP+) (Scholz *et al.*, 2000) into pBluescript II SK(-) (pBS) to make pBS-3×GFP. *INP1*-specific sequences comprising the 3′-end of the *INP1* gene and the start of its 3′-UTR were then added to the 5′- and 3′-ends of the 3×GFP sequence, respectively. The resulting plasmid was digested to release the integration cassette, which was used for transformation.

To construct an Inp1p-Tom22p chimera, a CORE-UK cassette in the 3′-end of the *INP1* gene was replaced by homologous recombination with a cassette containing the ORF of the *TOM22* gene flanked at its 5′-end with 60 nucleotides corresponding to the 3′-end of the *INP1* gene and at its 3′-end with 60 nucleotides corresponding to the start of the *INP1* 3′-UTR.

Strains expressing genomically integrated split-GFP chimeras were made by transforming cells harboring CORE-UK cassettes in the 3′-ends of the *INP1* and *PEX3* genes with cassettes coding for a 5′-polyglycine linker followed by in-frame sequences for N- and C-terminal fragments of GFP, respectively. GFP was split at residues Q157/K158 in the resulting *INP1*-½GFP and *PEX3*-½GFP chimeric genes.

Genomic site-directed mutagenesis of the *PEX3* gene was accomplished by first inserting a CORE-UK cassette at a locus of future mutagenesis, followed by its excision through transformation with 80-nucleotide integrative recombinant oligonucleotides harboring the desired point mutation and counterselection on 5-FOA. Introduced changes to the *PEX3* gene were confirmed by sequencing its entire ORF.

Strains expressing genomically integrated peroxisomal reporters were constructed by replacing the ORF of the *CAN1* locus with sequence coding for GFP+ or mCherry (Shaner *et al.*, 2004) fused at their C-termini to the peroxisome targeting signal 1 (PTS1), Ser-Lys-Leu, and selection by growth on SM-arg+can plates (Hampsey, 1997).

Image processing and quantitative image analysis

Acquired fluorescence images were deconvolved using algorithms provided by Huygens Professional Software (Scientific Volume Imaging BV, The Netherlands). 3D data sets were processed to remove noise and reassign blur through an iterative Classic Maximum Likelihood Estimation algorithm and an experimentally derived point spread function. The transmission image was treated differently. A Gaussian filter and blue color were applied to the transmission image using Imaris software (v.7.6.1) (Bitplane, South Windsor, CT). The level of the transmission image was modified, and the image was processed until only the circumference of the cell was visible. To prevent interference of internal structures captured in the transmission images, the internal structures were removed in Adobe Photoshop. Imaris software was then used to display the deconvolved 3D data set with the processed transmission image and to prepare the image files before final figure assembly in Adobe Photoshop and Adobe Illustrator (Adobe Systems, San Jose, CA).

Peroxisome inheritance was quantified in cells expressing the fluorescent peroxisomal reporter GFP-PTS1. Cells were grown to early exponential phase (OD_{600} = ~0.3) in YPD medium and visualized by confocal fluorescence microscopy. To capture all fluorescent peroxisomes, three optical sections were collected at a *z*-spacing of 1.6 μm using high detector gain. Images were flattened into maximum intensity projections, and all visibly budded cells were analyzed in a randomly chosen field. Budded cells were grouped into two size categories

based on bud volume (Fagarasanu *et al.*, 2009). Bud volume in small-budded and large-budded cells constituted 0-24% and 25-48%, respectively, of mother cell volume. Mother cells were scored using an all-or-none criterion for the presence or absence of fluorescent peroxisomes. Quantification was performed on at least 100 cells from each strain.

The contact area between peroxisomes and mitochondria or peroxisomes and the cER was computed using Imaris software. Surfaces representing peroxisomes as defined by GFP-PTS1 fluorescence, mitochondria as defined by Sdh2p-mCherry fluorescence, and cER as defined by Rtn1p-mCherry fluorescence were reconstructed using the "Surfaces" function and absolute intensity and automated threshold settings. The dataset was resampled to isotropic voxel size and converted to a 32 bit floating point. A distance transformation was applied to the mitochondrial or ER surface to extend outward and generate a new channel, "distance to mitochondria/ER". A mask was applied to the peroxisome surface to crop out all regions located outside of peroxisomes. The contact area was then determined as the region of overlap between peroxisomes and "distance to mitochondria/ER" using distance threshold settings between 0 and 0.1 μm. A surface bounding the overlapping voxels was created to count the number of voxels in the contact area. The contact area in μm^2 was calculated by multiplying the number of voxels and the cross sectional area of a single voxel. The overall contact area between peroxisomes and mitochondria or the cER was expressed as a percentage of the total peroxisome surface area.

Peroxisome speed in Movie 7 was computed using the "Spots" function of Imaris. After background subtraction, tracking was enabled for all spots defined by mCherry-PTS1 fluorescence with a diameter of 300 nm or greater and "quality" above automatic threshold settings. An autoregressive motion algorithm was applied to track individual peroxisomes. Only tracks lasting more than 75 s were considered for subsequent analysis. Track speed was displayed as color-coded

lines (red-green, 0-40 nm/s) in Figure 7C. To calculate the Inp1p content of individual peroxisomes, the ratio of the "intensity mean" of the green to the red channel was computed for each spot at each time point. Peroxisomes were subsequently categorized according to their track speed and plotted against their Inp1p content in Figure 7D.

Subcellular fractionation

Differential centrifugation was performed on cells grown in YPD medium to late exponential phase. Briefly, cells (5-6 g of wet cell weight) from 1 L of culture were washed and spheroplasted with 2 mg of Zymolase 100T per gram of cells in DTT buffer (10 mM DTT, 100 mM Tris-HCl, pH 9.4) for approximately 45 min at 30ºC. Spheroplasts were broken by homogenization in buffer H (0.6 M sorbitol, 2.5 mM MES, pH 5.5, 1 mM KCl, 1 mM EDTA, 1× complete protease inhibitors (Roche, Indianapolis, IN)). Cell debris and nuclei were pelleted from the homogenate by five successive centrifugations at 1,000 × *g* for 6 min each to generate a postnuclear supernatant (PNS), which was subsequently subjected to centrifugation at 20,000 × *g* for 35 min in a JS35.1 rotor (Beckman, Brea, CA) to yield supernatant (20kgS) and pellet (20kgP) fractions. The 20kgS fraction was subjected to a second round of centrifugation at 200,000 × *g* in a SW41 rotor (Beckman) for 2 h to yield 200kgS and 200kgP fractions. Equal amounts of protein from each fraction were analyzed by SDS-PAGE.

For flotation gradient centrifugation, PNS was prepared from 1 L of YPD-grown cells as described above. 2 ml of PNS were mixed 1:1 with a 68% (w/v) sucrose solution in buffer H and placed at the bottom of a SW41 centrifuge tube. The PNS was overlaid with 2 ml cushions of 25%, 18%, and 10% (w/v) sucrose in buffer H, followed by 1.5 ml of buffer H. The samples were subjected to centrifugation for 2 h at 150,000 × *g*, and 15 fractions of 0.75 ml each were collected from the top of the gradient. Equal portions of each fraction were analyzed by SDS-

PAGE. Subcellular fractionation of SCIM-incubated cells was done as described (Smith *et al.*, 2002). Fifty OD_{600} units of cells growing exponentially in YPD medium were seeded into 1 L of SCIM and grown for 15 h at 30ºC. A 20kgP fraction was prepared, and peroxisomes and mitochondria were separated by isopycnic density gradient centrifugation on Nycodenz gradients.

Assay for direct protein binding

Direct binding between Pex3p and Inp1p was examined essentially as described (Fagarasanu *et al.*, 2006). GST fusions of the cytosolic tail (a.a. 51-441) of Pex3p and Pex3p-V81E were constructed using pGEX4T-1 (GE Healthcare, Piscataway, NJ). MBP fusions to full-length Inp1p, as well as its N- and C-terminal domains (a.a. 1-280 and 280-420, respectively), were constructed using pMAL-c2 (New England Biolabs, Ipswich, MA). Recombinant proteins were expressed in the *E. coli* strain BL21 (Invitrogen). Purified MBP-Inp1p fusions or MBP alone were immobilized on amylose resin and incubated with 250 µg of *E. coli* lysate containing either a GST-fusion or GST alone in binding buffer (20 mM Tris-HCl, pH 7.5, 100 mM KCl, 5 mM $MgCl_2$, 0.5% (v/v) Triton X-100). To estimate the binding capacity of full-length Inp1p and its domains, purified MBP-Inp1p, MBP-Inp1p-N and MBP-Inp1p-C were each adjusted to a concentration of 10 µM and coupled to amylose resin. Aliquots of resin were incubated with serial dilutions of *E. coli* lysates containing either GST-Pex3p or GST-Pex3p-V81E in binding buffer. Unbound proteins were removed by washing five times in binding buffer. Immobilized proteins were eluted in sample buffer (50 mM Tris-HCl, pH 6.8, 2% SDS, 5% (v/v) glycerol, 0.002% bromophenol blue, 100 mM 2-mercaptoethanol) and subjected to SDS-PAGE and immunoblotting.

Antibodies

Inp1p-HA was detected with mouse monoclonal HA-probe F7 antibody (Santa Cruz Biotechnology, Santa Cruz, CA). Rabbit antibody to *S. cerevisiae* glucose-6-phosphate dehydrogenase (G6PDH) was from Sigma-Aldrich (St. Louis, MO). Rabbit antiserum to MBP was from New England Biolabs. GST was detected with mouse monoclonal antibody GST-2 (Sigma-Aldrich). Rabbit antiserum to *S. cerevisiae* Tom70p was kindly provided by Dr. Frank Nargang (University of Alberta). Antisera to *S. cerevisiae* Pex3p, Pot1p (thiolase), Nvy1p, and Sec61p have been described (Stirling *et al.*, 1992; Tam *et al.*, 2005; Ungermann *et al.*, 1998). IgGs to Pex3p were affinity-purified on immobilized recombinant Pex3p. Horseradish peroxidase-conjugated donkey anti-mouse and donkey anti-rabbit secondary antibodies were used to detect primary antibodies in immunoblot analysis. Antigen-antibody complexes in immunoblots were detected by enhanced chemiluminescence (GE Healthcare).

Modeling the structure of S. cerevisiae Pex3p

The crystal structure of the cytosolic tail of human Pex3p in complex with a short α-helical fragment of Pex19p (Sato *et al.*, 2010; Schmidt *et al.*, 2010) was used to model the structure of *S. cerevisiae* Pex3p using Rosetta 3.3 (Leaver-Fay *et al.*, 2011).

Supplementary Figure S1 Comparative alignment of the Pex19p-binding site of different Pex3p proteins. Identical residues are in black and conserved residues in grey. The tryptophan residue essential for interaction of human Pex3p with Pex19p (Sato *et al.*, 2008) is marked with an asterisk.

Supplementary Figure S2 Peroxisomes in a *vps1Δ/dnm1Δ/inp1Δ/inp2Δ* mutant distribute randomly between mother and daughter cells. A growing cell population was tracked over time. Insertion of a peroxisome into the bud is depicted by the arrow. Bar, 3 µm.

Supplementary Figure S3 High-level expression of the *INP1* gene leads to collapse of the peroxisomal compartment. (**A**, **B**) Cells expressing mCherry-PTS1 and either wild-type Pex3p (**A**) or Pex3p-V81E (**B**) were transformed with plasmids coding for Inp1p-GFP under the *INP1* promoter (low-level expression), the *CAN1* promoter (intermediate-level expression), or the *TEF* promoter (high-level expression). Overproduction of Inp1p from the *TEF* promoter causes peroxisome deficiency and mislocalization of mCherry-PTS1 to the cytosol in wild-type cells but not *pex3-V81E* cells. A wild-type cell that has apparently lost the plasmid can form peroxisomes (**A**, arrowheads). Clusters of cortically anchored peroxisomes are depicted by arrows (**A, B**). Left panels present merged images of the middle and right panels. Bar, 5 µm. (**C**) The wild-type and *pex3-V81E* strains above were transformed with plasmid coding for Inp1p-HA under control of the *INP1*, *CAN1*, or *TEF* promoter. Equal amounts of protein from whole cell lysates were separated by SDS-PAGE, and immunoblots were probed with antibodies against HA, Pex3p, and G6PDH.

Movie 1 (associated with Figure 1): Rotational model of *S. cerevisiae* Pex3p.

Movie 2 (associated with Figure 3): Dynamics of peroxisomes labeled by GFP-PTS1 and mitochondria labeled by Sdh2p-mCherry in *inp1Δ* cells containing either empty plasmid (top), plasmid expressing *INP1* (middle), or plasmid expressing a *TOM70-INP1* chimera (bottom).

Movie 3 (associated with Figure 3): Dynamics of peroxisomes and mitochondria in a strain constitutively expressing an *INP1-TOM22* chimeric gene.

Movie 4 (associated with Figure 3): Dynamics of peroxisomes and mitochondria in *inp1Δ/pex3-V81E* cells containing plasmid expressing either *INP1* (top) or *TOM70-INP1* (bottom).

Movie 5 (associated with Figure 5): Reconstitution of peroxisome tethering in a cell mating assay between mutants expressing either the ER-portion (*pex3-W128L*) or the peroxisomal portion (*pex3-V81E*) of the ER-peroxisome tether. Merged images of the green and red channels are presented at left, while the green channel only is presented at right.

Movie 6 (associated with Figure 6): 3D reconstruction of surfaces corresponding to peroxisomes (green), cER (red), and the contact area between both organelles (white). Presented from top to bottom are wild-type, *inp1Δ* and *pex3-V81E* cells, as in Figure 6A.

Movie 7 (associated with Figure 7): Dynamics of peroxisomes labeled by mCherry-PTS1 and Inp1p-3×GFP in wild-type (top) and *pex3-V81E* (bottom) cells.

Movies 8-10 (associated with Figure 8): Fate of individual peroxisomes in a peroxisome population tracked by photoconversion of a Pot1p-3×Dendra2 reporter. Merged images of the green and red channels are presented at top, while the red channel only is presented at bottom.

Table S1 *S. cerevisiae* strains used in this study

Strain	Genotype	Derivation
BY4741	*MATa*, *his3Δ1*, *leu2Δ0*, *met15Δ0*, *ura3Δ0*	(Giaever *et al.*, 2002)
BY4742	*MATα, his3Δ1*, *leu2Δ0, lys2Δ0, ura3Δ0*	(Giaever *et al.*, 2002)
HF7c	*MATa, ura3-52, his3-200, lys2-801, ade2-101, trp1-901, leu2-3, 112, gal4-542, gal80-538, LYS2::GAL1$_{UAS}$-GAL1$_{TATA}$-HIS3, URA3::(GAL 17mers) 3-Cyc1$_{TATA}$-lacZ*	(Feilotter *et al.*, 1994)
SFY526	*MATa, ura3-52, his3-200, ade2-101, lys2-801, trp1-901, leu2-3, 112, can^r, gal4-542, gal80-538, URA::GAL1$_{UAS}$-GAL1$_{TATA}$-lacZ*	(Harper *et al.*, 1993)
inp1Δ	*MATα, his3Δ1, leu2Δ0, lys2Δ0, ura3Δ0, inp1::KanMX4*	(Giaever *et al.*, 2002)
pex3Δ	*MATα, his3Δ1, leu2Δ0, lys2Δ0, ura3Δ0, pex3::KanMX4*	(Giaever *et al.*, 2002)
BY4742, GFP-PTS1	*MATα, his3Δ1*, *leu2Δ0, lys2Δ0, ura3Δ0, can1::GFP-PTS1*	This study
BY4742, pex3Δ, GFP-PTS1	*MATα, his3Δ1*, *leu2Δ0, lys2Δ0, ura3Δ0, pex3::KanMX4, can1::GFP-PTS1,*	This study
BY4742, pex3Δ, inp1Δ, GFP-PTS1	*MATα, his3Δ1*, *leu2Δ0, lys2Δ0, ura3Δ0, pex3::KanMX4, inp1::HIS3, can1::GFP-PTS1*	This study
BY4742, INP1-GFP, PEX3-mCherry	*MATα, his3Δ1*, *leu2Δ0, lys2Δ0, ura3Δ0, inp1::INP1-GFP (natR), pex3::PEX3-mCherry (URA3)*	This study
BY4742, INP1-GFP, PEX3-mCherry, pex19Δ	*MATα, his3Δ1*, *leu2Δ0, lys2Δ0, ura3Δ0, inp1::INP1-GFP (natR), pex3::PEX3-mCherry (URA3), pex19::HIS3*	This study
BY4742, INP1-GFP, mCherry-PTS1	*MATα, his3Δ1*, *leu2Δ0, lys2Δ0, ura3Δ0, inp1::INP1-GFP (natR), can1::mCherry-PTS1*	This study
BY4742, INP1-GFP, mCherry-PTS1, pex19Δ	*MATα, his3Δ1*, *leu2Δ0, lys2Δ0, ura3Δ0, inp1::INP1-GFP (natR), can1::mCherry-PTS1, pex19::HIS3*	This study
BY4742, INP1-GFP, RTN1-mCherry, pex19Δ	*MATα, his3Δ1*, *leu2Δ0, lys2Δ0, ura3Δ0, inp1::INP1-GFP (natR), rtn1::RTN1-mCherry (URA3), pex19::HIS3*	This study
BY4742, INP1-GFP, SEC13-mCherry, pex19Δ	*MATα, his3Δ1*, *leu2Δ0, lys2Δ0, ura3Δ0, inp1::INP1-GFP (natR), sec13::SEC13-mCherry (URA3), pex19::HIS3*	This study
BY4742, INP1-GFP, pex3V81E-mCherry	*MATα, his3Δ1*, *leu2Δ0, lys2Δ0, ura3Δ0, inp1::INP1-GFP (natR), pex3::pex3V81E-mCherry (URA3)*	This study
BY4742, INP1-GFP, pex3V81E, RTN1-mCherry	*MATα, his3Δ1*, *leu2Δ0, lys2Δ0, ura3Δ0, inp1::INP1-GFP (natR), pex3::pex3V81E, rtn1::RTN1-mCherry (URA3)*	This study

BY4742, INP1-GFP, pex3V81E, SEC13-mCherry	*MATα, his3Δ1, leu2Δ0, lys2Δ0, ura3Δ0, inp1::INP1-GFP (natR), pex3::pex3V81E, sec13::SEC13-mCherry (URA3)*	This study
BY4742, INP1-GFP, pex3V81E, PEX30-mCherry	*MATα, his3Δ1, leu2Δ0, lys2Δ0, ura3Δ0, inp1::INP1-GFP (natR), pex3::pex3V81E, pex30::PEX30-mCherry (URA3)*	This study
BY4742, INP1-GFP, pex3Δ	*MATα, his3Δ1, leu2Δ0, lys2Δ0, ura3Δ0, inp1::INP1-GFP (natR), pex3::KanMX4*	This study
BY4742, INP1-GFP, pex3V81E-mCherry, pex19Δ	*MATα, his3Δ1, leu2Δ0, lys2Δ0, ura3Δ0, inp1::INP1-GFP (natR), pex3::pex3V81E-mCherry (URA3), pex19::HIS3*	This study
BY4742, INP1-HA	*MATα, his3Δ1, leu2Δ0, lys2Δ0, ura3Δ0, inp1::INP1-HA (HIS3)*	This study
BY4742, INP1-HA, pex3Δ	*MATα, his3Δ1, leu2Δ0, lys2Δ0, ura3Δ0, inp1::INP1-HA (HIS3), pex3::KanMX4*	This study
BY4742, INP1-HA, pex3-V81E	*MATα, his3Δ1, leu2Δ0, lys2Δ0, ura3Δ0, inp1::INP1-HA (HIS3), pex3::pex3-V81E*	This study
BY4742, INP1-HA, pex3-V81E, pex19Δ	*MATα, his3Δ1, leu2Δ0, lys2Δ0, ura3Δ0, inp1::INP1-HA (HIS3), pex3::pex3-V81E, pex19::KanMX4*	This study
BY4742, GFP-PTS1, SDH2-mCherry, inp1Δ	*MATα, his3Δ1, leu2Δ0, lys2Δ0, ura3Δ0, can1::GFP-PTS1, sdh2::SDH2-mCherry (natR), inp1::HIS3*	This study
BY4742, GFP-PTS1, SDH2-mCherry, INP1-TOM22	*MATα, his3Δ1, leu2Δ0, lys2Δ0, ura3Δ0, can1::GFP-PTS1, sdh2::SDH2-mCherry (natR), inp1::INP1-TOM22*	This study
BY4742, GFP-PTS1, SDH2-mCherry, inp1Δ, pex3-V81E	*MATα, his3Δ1, leu2Δ0, lys2Δ0, ura3Δ0, can1::GFP-PTS1, sdh2::SDH2-mCherry (natR), inp1::HIS3, pex3::pex3-V81E*	This study
BY4741, INP1-GFP, mCherry-PTS1, pex3-W128L	*MATa, his3Δ1, leu2Δ0, met15Δ0, ura3Δ0, inp1::INP1-GFP (natR), can1::mCherry-PTS1, pex3::pex3-W128L*	This study
BY4742, INP1-GFP, mCherry-PTS1, pex3-V81E	*MATα, his3Δ1, leu2Δ0, lys2Δ0, ura3Δ0, inp1::INP1-GFP (natR), can1::mCherry-PTS1, pex3::pex3-V81E*	This study
BY4741, INP1-½GFP, mCherry-PTS1, pex3-W128L	*MATa, his3Δ1, leu2Δ0, met15Δ0, ura3Δ0, inp1::INP1-½GFP, can1::mCherry-PTS1, pex3::pex3-W128L*	This study
BY4742, mCherry-PTS1, pex3-V81E-½GFP	*MATα, his3Δ1, leu2Δ0, lys2Δ0, ura3Δ0, can1::mCherry-PTS1, pex3::pex3-V81E-½GFP*	This study
BY4742, GFP-PTS1, RTN1-mCherry	*MATα, his3Δ1, leu2Δ0, lys2Δ0, ura3Δ0, can1::GFP-PTS1, rtn1::RTN1-mCherry (URA3)*	This study

BY4742, GFP-PTS1, RTN1-mCherry, inp1Δ	*MATα, his3Δ1, leu2Δ0, lys2Δ0, ura3Δ0, can1::GFP-PTS1, rtn1::RTN1-mCherry (URA3), inp1:: HIS3*	This study
BY4742, GFP-PTS1, RTN1-mCherry, pex3-V81E	*MATα, his3Δ1, leu2Δ0, lys2Δ0, ura3Δ0, can1::GFP-PTS1, rtn1::RTN1-mCherry (URA3), pex3::pex3-V81E*	This study
BY4742, INP1-3×GFP, mCherry-PTS1	*MATα, his3Δ1, leu2Δ0, lys2Δ0, ura3Δ0, inp1::INP1-3×GFP, can1::mCherry-PTS1*	This study
BY4742, INP1-3×GFP, mCherry-PTS1, pex3-V81E	*MATα, his3Δ1, leu2Δ0, lys2Δ0, ura3Δ0, inp1::INP1-3×GFP, can1::mCherry-PTS1, pex3::pex3-V81E*	This study
BY4742, INP1-GFP, mCherry-PTS1, vps1Δ, dnm1Δ	*MATα, his3Δ1, leu2Δ0, lys2Δ0, ura3Δ0, inp1::INP1-GFP (natR), can1::mCherry-PTS1, vps1::HIS3, dnm1::URA3*	This study
BY4742, INP2-GFP, mCherry-PTS1, vps1Δ, dnm1Δ	*MATα, his3Δ1, leu2Δ0, lys2Δ0, ura3Δ0, inp2::INP2-GFP (natR), can1::mCherry-PTS1, vps1::HIS3, dnm1::URA3*	This study
BY4742, INP1-GFP, mCherry-PTS1, RTN1-mCerulean, vps1Δ, dnm1Δ	*MATα, his3Δ1, leu2Δ0, lys2Δ0, ura3Δ0, inp1::INP1-GFP (natR), can1::mCherry-PTS1, rtn1::RTN1-mCerulean (Hyg B), vps1::HIS3, dnm1::URA3*	This study
BY4742, INP2-GFP, mCherry-PTS1, RTN1-mCerulean, vps1Δ, dnm1Δ	*MATα, his3Δ1, leu2Δ0, lys2Δ0, ura3Δ0, inp2::INP2-GFP (natR), can1::mCherry-PTS1, rtn1::RTN1-mCerulean, vps1::HIS3, dnm1::URA3*	This study
BY4742, INP1-GFP, mCherry-PTS1, inp2Δ, vps1Δ, dnm1Δ	*MATα, his3Δ1, leu2Δ0, lys2Δ0, ura3Δ0, inp1::INP1-GFP (natR), can1::mCherry-PTS1, inp2::LEU2, vps1::HIS3, dnm1::URA3*	This study
BY4742, mCherry-PTS1, vps1Δ, dnm1Δ, inp1Δ, inp2Δ	*MATα, his3Δ1, leu2Δ0, lys2Δ0, ura3Δ0, can1::mCherry-PTS1, vps1::HIS3, dnm1::URA3, inp1::Hyg B, inp2::LEU2*	This study

Table S2 *pex3* point mutants used in this study

Mutation	**Reference**
V81E	This study
W128L	This study
N178D	This study
N188I	This study
N242D	This study
N247Y	This study
F353I	This study

Supplementary References

Fagarasanu A, Mast FD, Knoblach B, Jin Y, Brunner MJ, Logan MR, Glover JN, Eitzen GA, Aitchison JD, Weisman LS, Rachubinski RA (2009) Myosin-driven peroxisome partitioning in *S. cerevisiae*. *J Cell Biol* **186:** 541–554.

Feilotter HE, Hannon GJ, Ruddell CJ, Beach D (1994) Construction of an improved host strain for two hybrid screening. *Nucleic Acids Res* **22:** 1502–1503.

Giaever G, Chu AM, L. N, Connelly C, Riles L, Véronneau S, Dow S, Lucau-Danila A, Anderson K, André B, Arkin AP, Astromoff A, El-Bakkoury M, Bangham R, Benito R, Brachat S, Campanaro S, Curtiss M, Davis K, Deutschbauer A, Entian KD, Flaherty P, Foury F, Garfinkel DJ, Gerstein M, Gotte D, Güldener U, Hegemann JH, Hempel S, Herman Z, Jaramillo DF, Kelly DE, Kelly SL, Kötter P, LaBonte D, Lamb DC, Lan N, Liang H, Liao H, Liu L, Luo C, Lussier M, Mao R, Menard P, Ooi SL, Revuelta JL, Roberts CJ, Rose M, Ross-Macdonald P, Scherens B, Schimmack G, Shafer B, Shoemaker DD, Sookhai-Mahadeo S, Storms RK, Strathern JN, Valle G, Voet M, Volckaert G, Wang CY, Ward TR, Wilhelmy J, Winzeler EA, Yang Y, Yen G, Youngman E, Yu K, Bussey H, Boeke JD, Snyder M, Philippsen P, Davis RW, Johnston M (2002) Functional profiling of the *Saccharomyces cerevisiae* genome. *Nature* **418:** 387–391.

Hampsey M (1997) A review of phenotypes in *Saccharomyces cerevisiae*. *Yeast* **13:** 1099–1133.

Harper JW, Adami GR, Wei N, Keyomarsi K, Elledge SJ (1993) The p21 Cdk-interacting protein Cip1 is a potent inhibitor of G1 cyclin-dependent kinases. *Cell* **75:** 805–816.

Ishikawa K, Catlett NL, Novak JL, Tang F, Nau JJ, Weisman LS (2003) Identification of an organelle-specific myosin V receptor. *J Cell Biol* **160:** 887–897.

Leaver-Fay A, Tyka M, Lewis SM, Lange OF, Thompson J, Jacak R, Kaufman K, Renfrew DP, Smith CA, Sheffler W, Davis IW, Cooper S, Treuille A, Mandell DJ, Richter F, Ban YEA, Fleishman SJ, Corn JE, Kim DE, Lyskow S, Berrondo M, Mentzer S, Popovic Z, Havranek JJ, Karanicolas J, Das R, Meiler J, Kortemme T, Gray JJ, Kuhlman B, Baker D, Bradley P. (2011) ROSETTA3: an object-oriented software suite for the simulation and design of macromolecules. *Methods Enzymol* **487:** 545–574.

Longtine MS, McKenzie III A, Demarini DJ, Shah NG, Wach A, Brachat A, Philippsen P, Pringle JR (1998) Additional modules for versatile and economical PCR-based gene deletion and modification in *Saccharomyces cerevisiae*. *Yeast* **14:** 953–961.

Munck JM, Motley AM, Nuttall JM, Hettema EH (2009) A dual function for Pex3p in peroxisome formation and inheritance. *J Cell Biol* **187:** 463–471.

Rizzo MA, Springer GH, Granada B, Piston DW (2004) An improved cyan fluorescent protein variant useful for FRET. *Nat Biotechnol* **22:** 445–449.

Sato Y, Shibata H, Nakano H, Matsuzono Y, Kashiwayama Y, Kobayashi Y, Fujiki Y, Imanaka T, Kato H (2008) Characterization of the interaction between recombinant human peroxin Pex3p and Pex19p: identification of TRP-104 in Pex3p as a critical residue for the interaction. *J Biol Chem* **283:** 6136–6144.

Sato Y, Shibata H, Nakatsu T, Nakano H, Kashiwayama Y, Imanaka T, Kato H (2010) Structural basis for docking of peroxisomal membrane protein carrier Pex19p onto its receptor Pex3p. *EMBO J* **29:** 4083–4093.

Schmidt F, Treiber N, Zocher G, Bjelic S, Steinmetz MO, Kalbacher H, Stehle T, Dodt G (2010) Insights into peroxisome function from the structure of PEX3 in complex with a soluble fragment of PEX19. *J Biol Chem* **285:** 25410–25417.

Scholz O, Thiel A, Hillen W, Niederweiss M (2000) Quantitative analysis of gene expression with an improved green fluorescent protein. *Eur J Biochem* **267:** 1565–1570.

Shaner NC, Campbell RE, Steinbach PA, Giepmans BN, Palmer AE, Tsien RY (2004) Improved monomeric red, orange and yellow fluorescent proteins derived from *Discosoma* sp. red fluorescent protein. *Nat Biotechnol* **22:** 1567–1572.

Smith JJ, Marelli M, Christmas RH, Vizeacoumar FJ, Dilworth DJ, Ideker T, Galitski T, Dimitrov K, Rachubinski RA, Aitchison JD (2002) Transcriptome profiling to identify genes involved in peroxisome assembly and function. *J Cell Biol* **158:** 259–271.

Stirling CJ, Rothblatt J, Hosobuchi M, Deshaies R, Schekman R (1992) Protein translocation mutants defective in the insertion of integral membrane proteins into the endoplasmic reticulum. *Mol Biol Cell* **3:** 129–142.

Storici F, Resnick MA (2006) The *delitto perfetto* approach to *in vivo* site-directed mutagenesis and chromosome rearrangements with synthetic oligonucleotides in yeast. *Methods Enzymol* **409:** 329–345.

Tam YYC, Fagarasanu A, Fagarasanu M, Rachubinski RA (2005) Pex3p initiates the formation of a preperoxisomal compartment from a subdomain of the endoplasmic reticulum in *Saccharomyces cerevisiae*. *J Biol Chem* **280:** 34933–34939.

Ungermann C, Nichols BJ, Pelham HR, Wickner W (1998) A vacuolar v-t-SNARE complex, the predominant form in vivo and on isolated vacuoles, is disassembled and activated for docking and fusion. *J Cell Biol* **140:** 61–69.

Figure S1

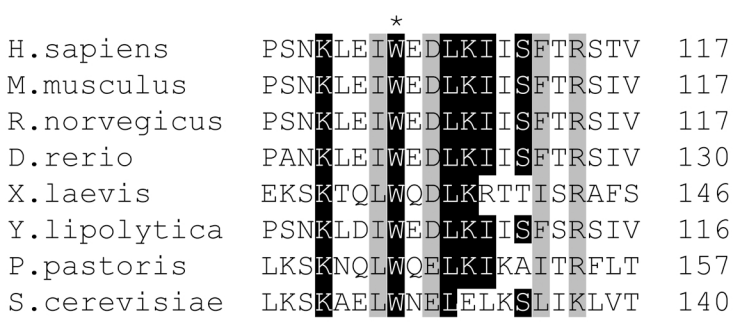
*
H.sapiens PSNKLEIWEDLKIISFTRSTV 117
M.musculus PSNKLEIWEDLKIISFTRSIV 117
R.norvegicus PSNKLEIWEDLKIISFTRSIV 117
D.rerio PANKLEIWEDLKIISFTRSIV 130
X.laevis EKSKTQLWQDLKRTTISRAFS 146
Y.lipolytica PSNKLDIWEDLKIISFSRSIV 116
P.pastoris LKSKNQLWQELKIKAITRFLT 157
S.cerevisiae LKSKAELWNELELKSLIKLVT 140

Figure S2

BY4742, mCherry-PTS1,
vps1Δ/dnm1Δ/inp1Δ/inp2Δ

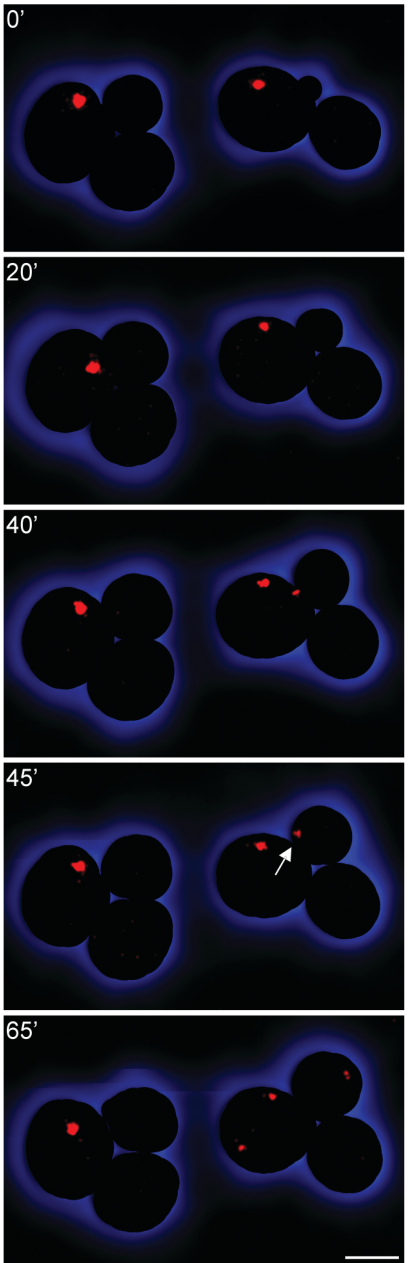

A

BY4742, *INP1*-GFP, mCherry-PTS1, *PEX3*

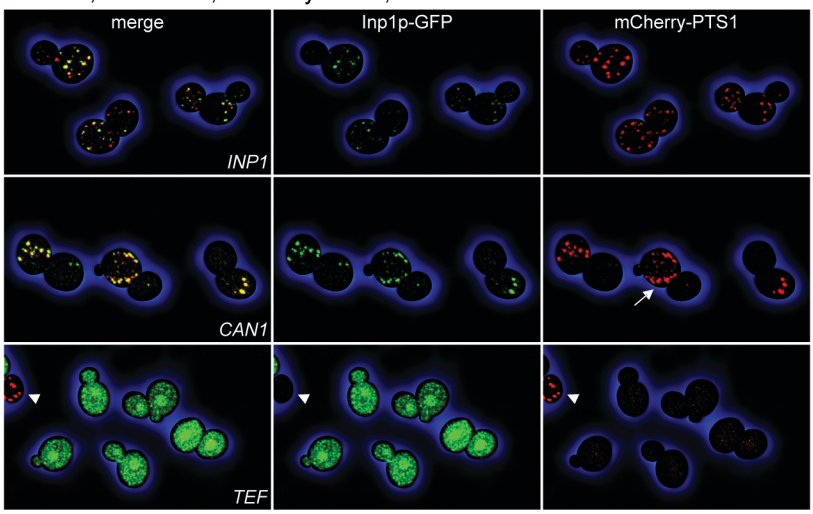

B

BY4742, *INP1*-GFP, mCherry-PTS1, *pex3-V81E*

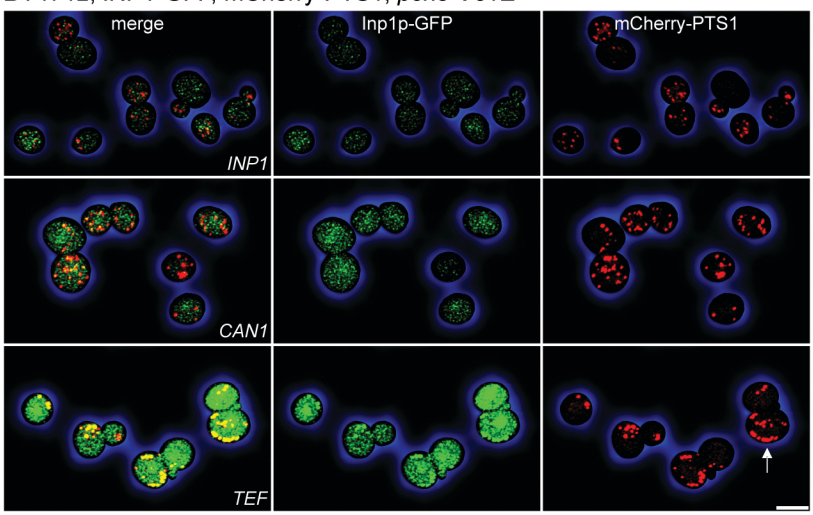

C